

Possible $\bar{D}^{(*)}\Xi_{cc}^{(*)}$ and $\Xi_{cc}^{(*)}\Xi_{cc}^{(*)}$ molecules as superflavor partners of T_{cc}

Manato Sakai*

Department of Physics, Nagoya University, Nagoya 464-8602, Japan

Yasuhiro Yamaguchi†

Department of Physics, Nagoya University, Nagoya 464-8602, Japan and

Kobayashi-Maskawa Institute for the Origin of Particles and the Universe, Nagoya University, Nagoya, 464-8602, Japan

(Dated: March 16, 2026)

The doubly charmed tetraquark T_{cc} has been reported by the LHCb experiment in 2022, and a lot of theoretical studies has been conducted. The small binding energy measured from $D^{*+}D^0$ threshold indicates that T_{cc} is a DD^* molecule. On the other hand, the superflavor symmetry, which relates heavy antiquarks to heavy diquarks, provides a useful framework for predicting the existence of partner exotic hadrons associated with T_{cc} . By replacing $\bar{D}^{(*)}$ with $\Xi_{cc}^{(*)}$ within this symmetry, $\bar{D}^{(*)}\Xi_{cc}^{(*)}$ and $\Xi_{cc}^{(*)}\Xi_{cc}^{(*)}$ are expected to form partner structures of T_{cc} . In this paper, we investigate bound and resonant states of $\bar{D}^{(*)}\Xi_{cc}^{(*)}$ and $\Xi_{cc}^{(*)}\Xi_{cc}^{(*)}$ based on the one boson exchange potential, where π , ρ , ω and σ are considered as bosons. The cutoff parameter and the coupling constants for $\bar{D}^{(*)}\Xi_{cc}^{(*)}$ and $\Xi_{cc}^{(*)}\Xi_{cc}^{(*)}$ are taken to be the same as those for T_{cc} due to superflavor symmetry. We also discuss the σ coupling constant, which is uncertain, dependence of these mass spectra. A lot of bound and resonant states with some quantum numbers are obtained for each σ coupling constant, but these mass spectra depend on the σ coupling constant significantly.

I. INTRODUCTION

Recently, in the heavy quark sector, numerous exotic hadrons have been reported by some experiments such as Belle, LHCb, BABAR, BESIII, and so on [1–13]. An exotic hadron is a hadron that cannot be accommodated within the conventional qqq and $q\bar{q}$ quark configurations. Most of the exotic hadrons are considered to be multiquark systems, but these spacial configurations are not obvious. On the other hand, most exotic hadrons are found slightly below a threshold, thus these states are analyzed as loosely bound states by the molecular model [14, 15].

Hadron-hadron interactions are one of the remaining problems in the hadron physics. The interaction between hadrons are described using the effective model such as the one boson exchange potential [16, 17] and quark-cluster model [18–21], or Lattice QCD calculation [22–25]. One of the “well-known” hadron-hadron interactions is the one pion exchange potential (OPEP) between nucleons. The OPEP is a long-range interaction and plays a crucial role in binding a deuteron which is a loosely bound state of a neutron and proton with $I(J^P) = 0(1^+)$. In the deuteron system, the tensor force of the OPEP which induces the $S - D$ mixing provides a crucial attraction between nucleons. On the other hand, other boson exchange potentials play a important role in middle or short ranges. For instance, the one ρ and ω exchange potentials are middle-range forces. In addition, the one σ exchange potential also provides the middle range forces, but this mechanism has not been understood completely. In fact,

this coupling constant is not determined.

Symmetries related to heavy quarks play an important role in exotic hadrons composed of heavy quarks. In particular, two symmetries are relevant: the heavy quark symmetry (HQS) [26–28] and the superflavor symmetry, also referred to as the heavy quark–antidiquark symmetry [29–31]. In the heavy quark limit, the spin-spin interaction of heavy quarks is suppressed at order $\mathcal{O}(1/m_Q)$. As a consequence, the heavy quark spin is conserved, leading to the emergence of the HQS. At the hadron level, the HQS leads to an approximate mass degeneracy between heavy hadrons with different spins. For example, the mass difference between the charmed pseudoscalar meson D and charmed vector meson D^* is about 140 MeV, which reflects the approximate mass degeneracy between these charmed hadrons. This mass degeneracy induces coupled channel effects such as $DD - DD^* - D^*D^*$ mixing. This mixing provides the one pion exchange potential which is prohibited in the $DD\pi$ vertex because of the parity conservation. The superflavor symmetry is a symmetry between a heavy antiquark, \bar{Q} , and a heavy diquark, QQ , both of which carry the same color representation $\mathbf{\bar{3}}_c$. Thus, one obtains the superflavor partner structure by replacing \bar{Q} with QQ in heavy hadrons. For instance, this symmetry establishes a partner structure between $\bar{D}(\bar{c}q)$ and $\Xi_{cc}(ccq)$. Since light mesons are coupled to the light quarks in the heavy hadrons, the superflavor symmetry allows us to use the same parameters for the interaction Lagrangians of $\bar{D}^{(*)}$ mesons and $\Xi_{cc}^{(*)}$ baryons.

One of the attractive exotic hadrons is the doubly charmed tetraquark T_{cc} reported by the LHCb experiment, and this state is considered to be an isoscalar state with spin-parity $J^P = 1^+$ [10, 11]. The quark content of T_{cc} is $cc\bar{u}\bar{d}$, and this state is a genuine ex-

* msakai@hken.phys.nagoya-u.ac.jp

† yamaguchi@hken.phys.nagoya-u.ac.jp

otic hadron because its quantum number, namely charm number 2 and baryon number 0, cannot be reached in the ordinary meson and baryon pictures. Moreover, T_{cc} lies very close to the $D^0 D^{*+}$ threshold. In fact, the mass difference δm measured from the corresponding threshold, is obtained as $\delta m = -273$ keV from the Breit–Wigner amplitude [10], while the pole analysis gives $\delta m = -360$ keV [11]. This observation implies that this state is a DD^* molecule. Consequently, a lot of studies based on the hadronic molecular model have been performed using the effective model in Refs. [14, 32–40] and the Lattice QCD in Refs. [25, 41–43]. We have studied T_{cc} as a $D^{(*)}D^{(*)}$ molecule within the coupled channel framework, motivated by the small mass differences between D and D^* mesons in Ref. [39]. In our analysis, we employed the one boson exchange potential (OBEP), where the π , ρ , ω and σ mesons are exchanged.

As mentioned before, the doubly charmed baryons $\Xi_{cc}^{(*)}$ are superflavor partners of the charmed mesons $\bar{D}^{(*)}$. Accordingly, in this study we consider the meson-baryon molecule $\bar{D}^{(*)}\Xi_{cc}^{(*)}$ and baryon-baryon molecule $\Xi_{cc}^{(*)}\Xi_{cc}^{(*)}$ as a superflavor partner of T_{cc} . Analogous to the analysis of T_{cc} , we employ the OBEP to describe the interactions in the $\bar{D}^{(*)}\Xi_{cc}^{(*)}$ and $\Xi_{cc}^{(*)}\Xi_{cc}^{(*)}$ molecules, and predict bound and resonant states. Furthermore, we use the same set of parameters such as coupling constants and a cutoff parameter as those adopted in the T_{cc} analysis as dictated by the superflavor symmetry. Here, we also consider the dependence of a sigma coupling constant.

This paper is organized as follows. In Sec. II, we introduce the formalism of the OBEP. In Sec. III, we show the

bound and resonant states of $\bar{D}^{(*)}\Xi_{cc}^{(*)}$ and $\Xi_{cc}^{(*)}\Xi_{cc}^{(*)}$. We also discuss the mass spectra of $\bar{D}^{(*)}\Xi_{cc}^{(*)}$ and $\Xi_{cc}^{(*)}\Xi_{cc}^{(*)}$ depending on the coupling constant of a σ meson. Finally, in Sec. IV, we summarize our results and discussions.

II. FORMALISM

In this study, we analyze bound and resonant states of $\bar{D}^{(*)}\Xi_{cc}^{(*)}$ and $\Xi_{cc}^{(*)}\Xi_{cc}^{(*)}$ based on the OBEP under the HQS and superflavor symmetry. In order to construct the Lagrangians between a heavy meson and a light boson, we introduce the anti-heavy meson field H^a , which is a linear combination of the anti-heavy pseudoscalar meson field \bar{D} and anti-heavy vector meson field \bar{D}^* [38, 44]:

$$H^a = [\bar{D}_\mu^{a*}\gamma^\mu - \bar{D}^a\gamma_5] \frac{1 - \not{v}}{2}, \quad (1)$$

where a is an isospin index and v is the four velocity with $v^0 > 0$ and $v^2 = 1$. This conjugate field is defined as

$$\bar{H}_a = \gamma^0 H^{a\dagger} \gamma^0 = \frac{1 - \not{v}}{2} [\bar{D}_{a\mu}^{*\dagger}\gamma^\mu - \bar{D}_a^\dagger\gamma_5]. \quad (2)$$

Using these fields, we construct the effective Lagrangians between the heavy meson and the pion, vector mesons (ρ , ω) and σ mesons, which are invariant under the $SU(2)$ flavor and heavy quark spin symmetries [38, 45]:

$$\begin{aligned} \mathcal{L}_H^\pi &= ig \text{tr} [\bar{H}^a \gamma_\mu \gamma_5 A^{\mu ab} H^b] \\ &= \frac{g}{f_\pi} (\bar{D}_a^{*\mu\dagger} \bar{D}_b + \bar{D}_a^\dagger \bar{D}_b^{*\mu}) \partial_\mu (\vec{\pi} \cdot \vec{\tau})_{ba} - i \frac{g}{f_\pi} \epsilon^{\mu\nu\rho\sigma} v_\mu \bar{D}_{a\nu}^{*\dagger} \bar{D}_{b\rho}^* \partial_\sigma (\vec{\pi} \cdot \vec{\tau})_{ba}, \end{aligned} \quad (3)$$

$$\begin{aligned} \mathcal{L}_H^v &= i\beta \text{tr} [\bar{H}^a v^\mu (\rho_\mu)^{ab} H^b] + i\lambda \text{tr} [\bar{H}^a \sigma^{\mu\nu} F_{\mu\nu}(\rho)^{ab} H^b] \\ &= \sqrt{2}\beta g_V \bar{D}^b \bar{D}^{a\dagger} v_\alpha \hat{\rho}^{a\alpha} 2\sqrt{2}\lambda g_V \epsilon^{\mu\nu\alpha\beta} (\bar{D}_\nu^{*\dagger} \bar{D} + \bar{D}^\dagger \bar{D}_\nu^*) \partial_\alpha \hat{\rho}_\beta - \sqrt{2}\beta g_V \bar{D}_\mu^{*\dagger} v \cdot \rho \bar{D}^{*\mu} + 2\sqrt{2}i\lambda g_V \bar{D}_\mu^* \bar{D}_\nu^{*\dagger} (\partial^\mu \hat{\rho}^\nu - \partial^\nu \hat{\rho}^\mu), \end{aligned} \quad (4)$$

$$\begin{aligned} \mathcal{L}_H^\sigma &= g_\sigma \text{tr} [\bar{H} \sigma H] \\ &= 2g_\sigma \bar{D}^{*\dagger} \cdot \bar{D}^* \sigma - 2g_\sigma \bar{D}^\dagger \bar{D} \sigma. \end{aligned} \quad (5)$$

Here, $f_\pi = 93$ MeV denotes the pion decay constant. The axial current A^μ and pseudoscalar field $\vec{\pi}$ are defined as

$$A^\mu = \frac{i}{2} (\xi^\dagger \partial^\mu \xi - \xi \partial^\mu \xi^\dagger), \quad \xi = \exp \left(i \frac{\vec{\pi} \cdot \vec{\tau}}{2f_\pi} \right), \quad (6)$$

$$\vec{\pi} \cdot \vec{\tau} = \begin{pmatrix} \pi^0 & \sqrt{2}\pi^+ \\ \sqrt{2}\pi^- & -\pi^0 \end{pmatrix}. \quad (7)$$

The field strength tensor and vector field are also defined

as

$$F_{\mu\nu}(\rho) = \partial_\mu \rho_\nu - \partial_\nu \rho_\mu - [\rho_\mu, \rho_\nu], \quad (8)$$

$$\rho_\mu = i \frac{g_V}{\sqrt{2}} \hat{\rho}_\mu, \quad (9)$$

$$\hat{\rho}_\mu = \frac{1}{\sqrt{2}} \begin{pmatrix} \rho^0 + \omega & \sqrt{2}\rho^+ \\ \sqrt{2}\rho^- & -\rho^0 + \omega \end{pmatrix}_\mu = \frac{1}{\sqrt{2}} (\vec{\tau} \cdot \vec{\rho}_\mu + \omega_\mu \mathbf{1}), \quad (10)$$

where $g_V = m_\rho / \sqrt{2} f_\pi$ is the coupling constant of a vector

meson.

We also introduce the superfield for the heavy baryon, ψ^μ , written as a linear combination of the doubly heavy baryon fields $\mathcal{B}(\frac{1}{2}^+)$ and $\mathcal{B}^{*\mu}(\frac{3}{2}^+)$ [38]:

$$\psi^\mu = \mathcal{B}^{*\mu} + \sqrt{\frac{1}{3}}(\gamma^\mu + v^\mu)\gamma_5\mathcal{B}. \quad (11)$$

Its conjugate field $\bar{\psi}^\mu$ is given by

$$\bar{\psi}^\mu = \bar{\mathcal{B}}^{*\mu} - \sqrt{\frac{1}{3}}\bar{\mathcal{B}}\gamma_5(\gamma^\mu + v^\mu). \quad (12)$$

Here, \mathcal{B} and \mathcal{B}^* denote the Dirac spinor and Rarita-Schwinger spinor, which satisfy the constraints $\mathcal{B}^{(*)} = \frac{1+\not{v}}{2}\mathcal{B}^{(*)}$, respectively.

Under the superflavor symmetry, the effective interaction Lagrangians for the doubly heavy baryon with the pion, vector mesons, and the σ meson are obtained as:

$$\begin{aligned} \mathcal{L}_\psi^\pi &= ig\bar{\psi}^\mu\gamma_\nu\gamma_5A^\nu\psi_\mu \\ &= -\frac{g}{2f_\pi}\bar{\mathcal{B}}^{*\mu}\partial_\nu(\vec{\pi}\cdot\vec{\tau})\gamma^\nu\gamma_5\mathcal{B}_\mu + \sqrt{\frac{1}{3}}\frac{g}{f_\pi}(\bar{\mathcal{B}}^{*\mu}\partial_\mu(\vec{\pi}\cdot\vec{\tau})\mathcal{B} + \bar{\mathcal{B}}\partial_\mu(\vec{\pi}\cdot\vec{\tau})\mathcal{B}^{*\mu}) - \frac{g}{6f_\pi}\bar{\mathcal{B}}\partial_\nu(\vec{\pi}\cdot\vec{\tau})\gamma^\nu\gamma_5\mathcal{B} \end{aligned} \quad (13)$$

$$\begin{aligned} \mathcal{L}_\psi^v &= i\beta\bar{\psi}^\mu v\cdot\rho\psi_\mu + i\lambda\bar{\psi}^\mu\sigma^{\alpha\beta}F_{\alpha\beta}(\rho)\psi_\mu \\ &= -\frac{\beta g_V}{\sqrt{2}}(\bar{\mathcal{B}}^{*\mu}v\cdot\hat{\rho}\mathcal{B}_\mu^* - \bar{\mathcal{B}}v\cdot\hat{\rho}\mathcal{B}) - i\frac{\lambda g_V}{\sqrt{2}}\bar{\mathcal{B}}^{*\mu}\gamma_\alpha\gamma_\beta(\partial^\alpha\hat{\rho}^\beta - \partial^\beta\hat{\rho}^\alpha)\mathcal{B}_\mu^* \\ &\quad + i2\sqrt{\frac{2}{3}}\lambda\bar{\mathcal{B}}_\alpha^*\gamma_\beta\gamma_5(\partial^\alpha\hat{\rho}^\beta - \partial^\beta\hat{\rho}^\alpha)\mathcal{B} + i2\sqrt{\frac{2}{3}}\lambda\bar{\mathcal{B}}\gamma_\alpha\gamma_5(\partial^\alpha\hat{\rho}^\beta - \partial^\beta\hat{\rho}^\alpha)\mathcal{B}_\beta^* - i\frac{\lambda}{3\sqrt{2}}\bar{\mathcal{B}}\gamma_\alpha\gamma_\beta(\partial^\alpha\hat{\rho}^\beta - \partial^\beta\hat{\rho}^\alpha)\mathcal{B} \end{aligned} \quad (14)$$

$$\begin{aligned} \mathcal{L}_\psi^\sigma &= g_\sigma\bar{\psi}^\mu\sigma\psi_\mu \\ &= -g_\sigma\bar{\mathcal{B}}_{QQ}\sigma\mathcal{B}_{QQ} + g_\sigma\bar{\mathcal{B}}_{QQ}^*\sigma\mathcal{B}_{QQ}^*. \end{aligned} \quad (15)$$

We note that the coupling constants in $\mathcal{L}_\psi^{\text{boson}}$ are the same with those in $\mathcal{L}_H^{\text{boson}}$ owing to the superflavor symmetry.

The potential in the momentum space is expressed in terms of the scattering amplitude $i\mathcal{M}$ for the t -channel Feynman diagram as

$$V(q) = i\frac{i\mathcal{M}}{\sqrt{\prod_i 2m_i \prod_f 2m_f}}, \quad (16)$$

where $m_{i(f)}$ are the masses of the initial (final) states. When the Fourier transformation is implemented, the dipole-type form factor is attached to each vertex in order

to take account for the hadronic size:

$$F(\vec{q}; m_{\text{ex}}) = \frac{\Lambda^2 - m_{\text{ex}}^2}{\Lambda^2 + \vec{q}^2}, \quad (17)$$

where Λ and m_{ex} are the cutoff parameter and the mass of the exchanged meson, respectively. \vec{q} is a momentum transfer carried by the exchanged meson. Following these procedures, the OBEPs are obtained. In particular, the one pion exchange potentials are given as

$$\begin{aligned} V^\pi(r) &= k_\pi \frac{1}{3} \left(\frac{g}{2f_\pi} \right)^2 \left[\vec{\mathcal{O}}_1 \cdot \vec{\mathcal{O}}_2 C(r; m_\pi) + S_{12}(\hat{r}) T(r; m_\pi) \right] \vec{\tau}_1 \cdot \vec{\tau}_2, \end{aligned} \quad (18)$$

where k_π is a constant depending on the process, and $C(r; m_\pi)$ and $T(r; m_\pi)$ are the central and tensor potentials, respectively:

$$C(r; m_{\text{ex}}) = \frac{m_{\text{ex}}^2}{4\pi} \left[\frac{e^{-m_{\text{ex}}r}}{r} - \frac{e^{-\Lambda r}}{r} - \frac{\Lambda^2 - m_{\text{ex}}^2}{2\Lambda} e^{-\Lambda r} \right], \quad (19)$$

$$T(r; m_{\text{ex}}) = \frac{1}{4\pi} \left[(3 + 3m_{\text{ex}}r + m_{\text{ex}}^2 r^2) \frac{e^{-m_{\text{ex}}r}}{r^3} - (3 + 3\Lambda r + \Lambda^2 r^2) \frac{e^{-\Lambda r}}{r^3} + \frac{m_{\text{ex}}^2 - \Lambda^2}{2} (1 + \Lambda r) \frac{e^{-\Lambda r}}{r} \right]. \quad (20)$$

TABLE I. Coupling constants of the effective Lagrangians [33, 46–50]. $g_{\sigma NN}$ is a coupling constant between a σ meson and a nucleon, while g_π is determined by the Goldberger-Treiman relation.

Coupling constants	Values	
g	0.59	$D^* \rightarrow D\pi$ decay
β	0.9	Lattice QCD
λ	0.56 GeV^{-1}	B meson decay
g_σ^L	3.4	$g_{\sigma NN}/3$
g_σ^S	0.76	$g_\pi/2\sqrt{6}$

TABLE II. Masses of heavy hadrons and light mesons [52]. The values are given in units of MeV.

Heavy hadron	Values [MeV]	Light meson	Values [MeV]
\bar{D}	1868 MeV	π	138 MeV
\bar{D}^*	2009 MeV	ρ	770 MeV
Ξ_{cc}	3621 MeV	ω	782 MeV
Ξ_{cc}^*	3727 MeV	σ	500 MeV

We note that the energy transfer at the vertex is neglected, and the contact term, which represents the short range potential, is removed because the one light-boson exchange potentials are the long or middle range potentials. In addition, \vec{O} denotes the spin operators of the charmed meson or the doubly charmed baryon, and $S_{12}(\hat{r})$ is the tensor operator.

Finally, the parameters are summarized in Table. I. The pion coupling constant g is determined by the $D^* \rightarrow D\pi$ decay [46], and β and λ are determined by the Lattice QCD and B meson decay [47, 48], respectively. The coupling constant g_σ is uncertain, but there are two typical values. The large g_σ denoted by g_σ^L is determined by $g_{\sigma NN}/3$ with $g_{\sigma NN}$ being the coupling constant of a σ meson and a nucleon [48]. On the other hand, the small g_σ denoted by g_σ^S is determined by $g_\pi/2\sqrt{6}$ with g_π determined the Goldberger-Treiman relation [33, 49, 50].

We also summarize the hadron masses in table II. The isospin symmetry is assumed for the masses of the heavy meson \bar{D} and pion π . Moreover, the mass of Ξ_{cc}^* , which has not yet been observed, is determined using the relation derived from the superflavor symmetry [51]:

$$m_{\Xi_{cc}^*} - m_{\Xi_{cc}} = \frac{3}{4}(m_{D^*} - m_D). \quad (21)$$

III. NUMERICAL CALCULATION

In this section, we investigate the bound and resonant states of $\bar{D}^{(*)}\Xi_{cc}^{(*)}$ and $\Xi_{cc}^{(*)}\Xi_{cc}^{(*)}$ with dependence on g_σ .

First, the cutoff parameter Λ is determined to reproduce the binding energy of T_{cc} , 340 keV, for both

cases of g_σ^L and g_σ^S by solving the coupled channel Schrödinger equation [39] using the Gaussian expansion method [53, 54]. We find that $\Lambda_L = 1074.6 \text{ MeV}$ for g_σ^L and $\Lambda_S = 1682.4 \text{ MeV}$ for g_σ^S reproduce the binding energy of T_{cc} . In the case of g_σ^L , the σ exchange force plays a major role in binding T_{cc} , as discussed in Ref. [38, 39]. For case g_σ^S , however, the contribution of the σ exchange becomes weaker. As a result, a larger cutoff parameter is required for g_σ^S than for g_σ^L , which indicates that the one π and one ρ exchange forces provide stronger contributions [38].

A. $\bar{D}^{(*)}\Xi_{cc}^{(*)}$ molecule

In this subsection, we show the numerical results for $\bar{D}^{(*)}\Xi_{cc}^{(*)}$ with $J^P = \frac{1}{2}^-, \frac{3}{2}^-$ and $\frac{5}{2}^-$ for $I = 0, 1$. We solve the coupled-channel Schrödinger equation by the Gaussian expansion method and complex scaling method [55–57]. The channels for $\bar{D}^{(*)}\Xi_{cc}^{(*)}$ with the corresponding spin-parity J^P are listed in Table. III. The mass spectra of the isoscalar $\bar{D}^{(*)}\Xi_{cc}^{(*)}$ with $g_\sigma = g_\sigma^L$ and $g_\sigma = g_\sigma^S$ are depicted in Fig. 1, while the numerical results for both the isoscalar and isovector $\bar{D}^{(*)}\Xi_{cc}^{(*)}$ are summarized in Table IV. These results indicate the appearance of bound and resonant states in the $\bar{D}^{(*)}\Xi_{cc}^{(*)}$ system with $J^P = \frac{1}{2}^-, \frac{3}{2}^-$ and $\frac{5}{2}^-$.

First, we find the bound states of $\bar{D}^{(*)}\Xi_{cc}^{(*)}$ with $0(\frac{1}{2}^-)$ which were also discussed in Ref. [38]. As shown in Table III, the S -wave $\bar{D}\Xi_{cc}$ component is present only in the $J^P = \frac{1}{2}^-$ state. This fact indicates the absence of bound states with $J^P = \frac{3}{2}^-$ and $\frac{5}{2}^-$, because a strong attraction is required to produce a bound state for $L \neq 0$. The wavefunctions of $\bar{D}^{(*)}\Xi_{cc}^{(*)}$ with $0(\frac{1}{2}^-)$ are shown in Fig. 2, and their binding energies, mixing ratios and root mean squared (r.m.s) distances are summarized in Table V. The binding energy of $\bar{D}^{(*)}\Xi_{cc}^{(*)}$ with $g_\sigma = g_\sigma^S$ is larger than that with $g_\sigma = g_\sigma^L$. In the both cases, the $\bar{D}\Xi_{cc}(^2S)$ is dominant to bind $\bar{D}^{(*)}\Xi_{cc}^{(*)}$. However, as for the other channels, the composition of the mixing ratios differs between the two g_σ cases. In order to clarify these differences, we examine the g_σ dependence of the expectation value of the Hamiltonian (which corresponds to the binding energy) as well as those of one boson exchange potential as shown in Fig. 3. Here, the cutoff parameter is tuned to reproduce the binding energy of T_{cc} for each value of g_σ . As g_σ decreases, the expectation value of the one σ exchange potential becomes weaker, whereas those of the one π and one ρ exchange potentials become larger, reflecting the increase of the cutoff parameter Λ . Consequently, the effects of the tensor force from the one π exchange potential and the central force from the one ρ exchange potential are enhanced. This leads to a larger binding energy for the $\bar{D}^{(*)}\Xi_{cc}^{(*)}$ system with $g_\sigma = g_\sigma^S$ than for that with $g_\sigma = g_\sigma^L$, and enhances

TABLE III. Channels of $\bar{D}^{(*)}\Xi_{cc}^{(*)}$ with spin-parity J^P [38]. We use the notation $^{2S+1}L_J$ with S , L , and J being the spin, angular momentum and total momentum, respectively.

J^P	Channels
$\frac{1}{2}^-$	$\bar{D}\Xi_{cc}(^2S_{1/2}), \bar{D}\Xi_{cc}^*(^4D_{1/2}), \bar{D}^*\Xi_{cc}(^2S_{1/2}, ^4D_{1/2}), \bar{D}^*\Xi_{cc}^*(^2S_{1/2}, ^4D_{1/2}, ^6D_{1/2})$
$\frac{3}{2}^-$	$\bar{D}\Xi_{cc}(^2D_{3/2}), \bar{D}\Xi_{cc}^*(^4S_{3/2}, ^4D_{3/2}), \bar{D}^*\Xi_{cc}(^2D_{3/2}, ^4S_{3/2}, ^4D_{3/2}), \bar{D}^*\Xi_{cc}^*(^2D_{3/2}, ^4S_{3/2}, ^4D_{3/2}, ^6D_{3/2}, ^6G_{3/2})$
$\frac{5}{2}^-$	$\bar{D}\Xi_{cc}(^2D_{5/2}), \bar{D}\Xi_{cc}^*(^4D_{5/2}, ^4G_{5/2}), \bar{D}^*\Xi_{cc}(^2D_{5/2}, ^4D_{5/2}, ^4G_{5/2}), \bar{D}^*\Xi_{cc}^*(^2D_{5/2}, ^4D_{5/2}, ^4G_{5/2}, ^6S_{5/2}, ^6D_{5/2}, ^6G_{5/2})$

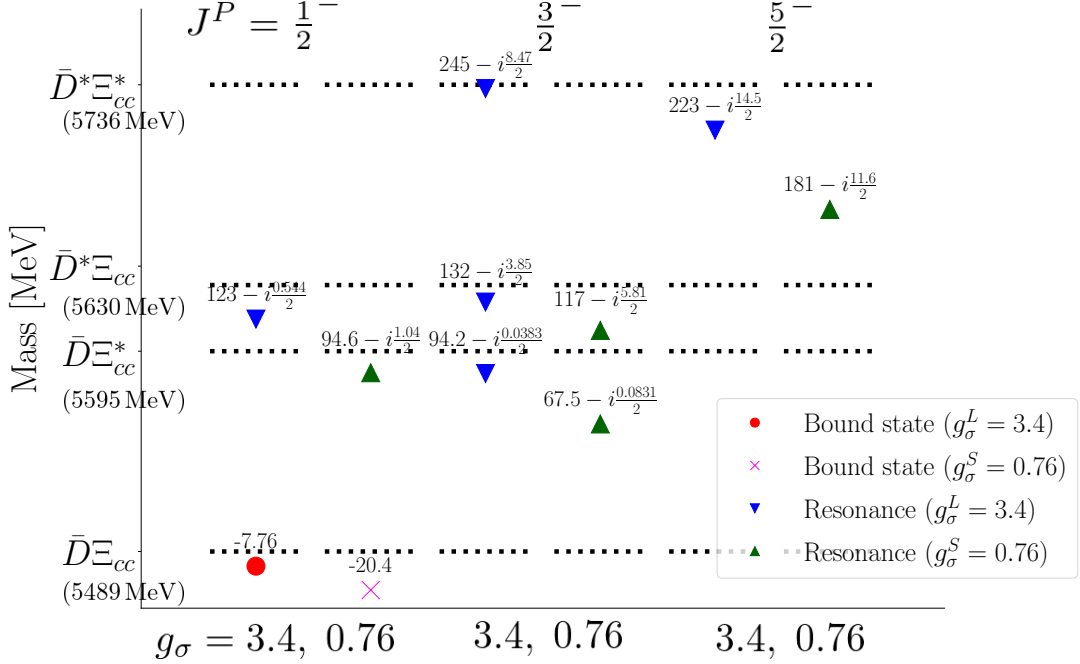


FIG. 1. Masses of the isoscalar $\bar{D}^{(*)}\Xi_{cc}^{(*)}$ with $\frac{1}{2}^-$, $\frac{3}{2}^-$ and $\frac{5}{2}^-$. The black dotted line shows the thresholds. The red circle and magenta cross show the masses of the bound states with g_σ^L and g_σ^S , respectively. The blue upward triangles and green downward triangles show the masses of the resonances with g_σ^L and g_σ^S , respectively. Numerical values displayed in the figure correspond to the eigenvalues $-B$ for bound states and $E_r - i\frac{\Gamma}{2}$ for resonances. The values are given in units of MeV.

the mixing between the $\bar{D}\Xi_{cc}(^2S)$ channel and the other channels.

It is instructive to compare the present analysis with previous study employing similar formalisms. In Ref. [38], bound states of $\bar{D}^{(*)}\Xi_{cc}^{(*)}$ were investigated within essentially the same formalism, except that the energy transfer at the vertex was taken into account. Nevertheless, our results are consistent with those of Ref. [38], indicating that the contributions from the energy transfer are small.

Next, we discuss the resonances of $\bar{D}^{(*)}\Xi_{cc}^{(*)}$ with $I = 0$. Resonances of $\bar{D}^{(*)}\Xi_{cc}^{(*)}$ are found not only for $J^P = \frac{1}{2}^-$ but also for $J^P = \frac{3}{2}^-$ and $\frac{5}{2}^-$. In higher-spin states, the larger number of $D^*\Xi_{cc}^*$ channels strengthens the coupled-channel dynamics, thereby promoting the emergence of resonant states. These states are indicated as Feshbach resonances because S -wave bound states of $\bar{D}^{(*)}\Xi_{cc}^{(*)}$ appear when the lower channels are cut. We obtain the resonance with $\frac{1}{2}^-$ below the $\bar{D}\Xi_{cc}$ threshold

for $g_\sigma = g_\sigma^S$, while this channel has no S -wave component. In fact, we find that the main component of the resonance is the $\bar{D}^*\Xi_{cc}(^2S)$ channel, and hence, it is originated from the $\bar{D}^*\Xi_{cc}(^2S)$ bound state. For $\frac{1}{2}^-$, we find no resonance below the $\bar{D}^*\Xi_{cc}$ threshold, while there is $\bar{D}^*\Xi_{cc}(^2S)$ channel. Actually, for $g_\sigma = g_\sigma^L$, a bound state appears when the lower channels are cut. However, the bound state disappears due to the level repulsion caused by coupling to the lower channels. Except for the quasi bound state of $\bar{D}^*\Xi_{cc}^*$ with $\frac{3}{2}^-$, the quasi bound states with $g_\sigma = g_\sigma^S$ are bound more deeply than those with $g_\sigma = g_\sigma^L$ for the same reason as in the case of the bound state. The absence of a quasi bound state of $\bar{D}^*\Xi_{cc}^*$ for $J^P = \frac{3}{2}^-$ with $g_\sigma = g_\sigma^S$ is attributed to the fact that the one π and one ρ exchange potentials do not provide sufficient attraction. Indeed, no bound state of $\bar{D}^*\Xi_{cc}^*$ with $J^P = \frac{3}{2}^-$ appears when the $\bar{D}\Xi_{cc}$, $\bar{D}\Xi_{cc}^*$, and $\bar{D}^*\Xi_{cc}$ channels are removed. In the similar way, a bound state with $\frac{1}{2}^-$ below the $\bar{D}^*\Xi_{cc}$ threshold is not found even if

TABLE IV. Eigenvalues of $\bar{D}^{(*)}\Xi_{cc}^{(*)}$. The first column shows $I(J^P)$ with I , J and P with the isospin, spin and parity, respectively. The third and fourth columns show the complex-scaled energy eigenvalues of the bound and resonant states for g_σ^L and g_σ^S , respectively. Here, $-B$ and E_r denote the masses measured from the lowest thresholds for bound states and resonances, respectively, and Γ represents the decay width of the resonances. The values are given in units of MeV.

$I(J^P)$ lowest threshold		$g_\sigma^L = 3.4$	$g_\sigma^S = 0.76$
		$-B, E_r - i\frac{\Gamma}{2}$	
$0(\frac{1}{2}^-)$	$\bar{D}\Xi_{cc}$	-7.76	-20.4
		$123 - \frac{0.544}{2}$	$94.6 - i\frac{1.04}{2}$
$1(\frac{1}{2}^-)$	$\bar{D}\Xi_{cc}$	$246 - i\frac{0.667}{2}$	-
		$94.2 - i\frac{0.0383}{2}$	$67.5 - i\frac{0.0831}{2}$
$0(\frac{3}{2}^-)$	$\bar{D}\Xi_{cc}$	$132 - i\frac{3.85}{2}$	$117 - i\frac{5.81}{2}$
		$245 - i\frac{8.47}{2}$	-
$0(\frac{5}{2}^-)$	$\bar{D}\Xi_{cc}$	$223 - i\frac{14.5}{2}$	$181 - i\frac{11.6}{2}$

TABLE V. The binding energy B , mixing ratios and root mean squared (r.m.s) distances of $\bar{D}^{(*)}\Xi_{cc}^{(*)}$ with $0(\frac{1}{2}^-)$ for each case of $g_\sigma = g_\sigma^L$ and $g_\sigma = g_\sigma^S$. The second and third columns show the properties in the case of $g_\sigma = 3.4$ and $g_\sigma = 0.76$, respectively. The values of the binding energy, mixing ratio, and r.m.s distance are given in units of MeV, %, and fm, respectively.

Properties	g_σ	
	$g_\sigma^L = 3.4$	$g_\sigma^S = 0.76$
B	7.76 MeV	20.4 MeV
$\bar{D}\Xi_{cc}(^2S)$	98.8 %	93.5 %
$\bar{D}\Xi_{cc}^*(^4D)$	0 %	0 %
$\bar{D}^*\Xi_{cc}(^2S)$	0.102 %	1.17 %
$\bar{D}^*\Xi_{cc}(^4D)$	0.135 %	0.377 %
$\bar{D}^*\Xi_{cc}^*(^2S)$	0.282 %	2.77 %
$\bar{D}^*\Xi_{cc}^*(^4D)$	0.0599 %	0.169 %
$\bar{D}^*\Xi_{cc}^*(^6D)$	0.582 %	2.01 %
r.m.s distance	1.40 fm	0.886 fm

the lower channels are ignored.

Finally, we consider the isovector $\bar{D}^{(*)}\Xi_{cc}^{(*)}$ state. We find a resonant state only for $I(J^P) = 1(\frac{1}{2}^-)$ with $g_\sigma = g_\sigma^L$, with a complex-scaled energy of $246 - i\frac{0.667}{2}$ MeV. The state is primarily bound by the one σ exchange potential. As discussed above, in the g_σ^S case, $\bar{D}^{(*)}\Xi_{cc}^{(*)}$ with $I = 0$ is bound mainly by the one π and one ρ exchange potentials. In contrast, for $I = 1$, the one π and one ρ exchange potentials provide weaker attractions because of the isospin factor $\vec{\tau}_1 \cdot \vec{\tau}_2$. Consequently, no $\bar{D}^{(*)}\Xi_{cc}^{(*)}$ state with $I = 1$ is obtained for $g_\sigma = g_\sigma^S$.

B. $\Xi_{cc}^{(*)}\Xi_{cc}^{(*)}$ molecule

In this subsection, we show the bound and resonant states of $\Xi_{cc}^{(*)}\Xi_{cc}^{(*)}$ with some quantum numbers. The channels of $\Xi_{cc}^{(*)}\Xi_{cc}^{(*)}$ are summarized in Table. VI. The numerical results for $\Xi_{cc}^{(*)}\Xi_{cc}^{(*)}$ are summarized in Fig. 4 and Table VII. In the similar way with the case of $\bar{D}^{(*)}\Xi_{cc}^{(*)}$, we obtain S -wave (quasi) bound states.

First, we discuss the bound states of $\Xi_{cc}^{(*)}\Xi_{cc}^{(*)}$ with $I(J^P) = 0(1^+)$. The wavefunctions of $\Xi_{cc}^{(*)}\Xi_{cc}^{(*)}$ with $0(1^+)$ are shown in Fig. 5, and their binding energies, mixing ratios and r.m.s distances are summarized in Table. VIII. As seen in $\bar{D}^{(*)}\Xi_{cc}^{(*)}$ with $0(\frac{1}{2}^-)$, the binding energy of $\Xi_{cc}^{(*)}\Xi_{cc}^{(*)}$ with $0(1^+)$ for $g_\sigma = g_\sigma^S$ is larger than for $g_\sigma = g_\sigma^L$. In both cases, the mixing ratio of $\Xi_{cc}^{(*)}\Xi_{cc}^{(*)}(^3S)$ is dominant, while that of the other channels differ between the cases of each g_σ . In order to clarify this dependence, we calculate the expectation values of the Hamiltonian and one boson exchange potentials, as shown in Fig. 6. As in the case of the bound state of $\bar{D}^{(*)}\Xi_{cc}^{(*)}$ with $0(\frac{1}{2}^-)$, the one σ exchange potential provides the strongest attraction for $g_\sigma = g_\sigma^L$, whereas for $g_\sigma = g_\sigma^S$ the dominant attraction arises from the one π and one ρ exchange potentials. In particular, the matrix elements $\langle \Xi_{cc}\Xi_{cc}(^3S) | V^\pi | \Xi_{cc}^*\Xi_{cc}^*(^7D) \rangle$ and $\langle \Xi_{cc}\Xi_{cc}(^3S) | V^\rho | \Xi_{cc}\Xi_{cc}(^3S) \rangle$ play important roles in binding $\Xi_{cc}^{(*)}\Xi_{cc}^{(*)}(0(1^+))$ with $g_\sigma = g_\sigma^S$. Moreover, the strength of $\langle \Xi_{cc}\Xi_{cc}(^3S) | V^\pi | \Xi_{cc}^*\Xi_{cc}^*(^7D) \rangle$ indicates that the $\Xi_{cc}^*\Xi_{cc}^*(^7D_1)$ component provides the third-largest contribution to the channel mixing.

We also discuss the bound states of $\Xi_{cc}^{(*)}\Xi_{cc}^{(*)}$ with $I = 1$. In this case, bound states of $\Xi_{cc}^{(*)}\Xi_{cc}^{(*)}$ with $1(0^+)$ and $1(1^+)$ are found, and their properties are discussed below. The mixing ratios of $\Xi_{cc}\Xi_{cc}(^1S_0)$ for $\Xi_{cc}^{(*)}\Xi_{cc}^{(*)}(1(0^+))$ and $[\Xi_{cc}\Xi_{cc}^*]_+(^3S_1)$ for $\Xi_{cc}^{(*)}\Xi_{cc}^{(*)}(1(1^+))$ are about 99%. This indicates that the one σ exchange potential provides the dominant attraction that is responsible for binding these states. On the other hand, for $g_\sigma = g_\sigma^S$, bound states of $\Xi_{cc}^{(*)}\Xi_{cc}^{(*)}$ with $I = 1$ are not obtained. This is because the one σ exchange potential becomes weaker for $g_\sigma = g_\sigma^S$ than for $g_\sigma = g_\sigma^L$, and the one π and one ρ exchange potentials cannot generate sufficient attractive force to bind $\Xi_{cc}^{(*)}\Xi_{cc}^{(*)}$ with $I = 1$.

Next, we discuss the resonances of $\Xi_{cc}^{(*)}\Xi_{cc}^{(*)}$. All resonances are identified as Feshbach resonances because bound states of the upper channels appear when the lower channels are cut. Moreover, most quasi bound states of $\Xi_{cc}\Xi_{cc}^*$ obtained with g_σ^S are bound more deeply than those obtained with g_σ^L for the same reasons as in the case of bound states of $\Xi_{cc}^{(*)}\Xi_{cc}^{(*)}$. However, no quasi bound state of $\Xi_{cc}\Xi_{cc}^*$ with $I(J^P) = 0(1^+)$ is found for $g_\sigma = g_\sigma^S$. This is because the one σ exchange potential is weaker for $g_\sigma = g_\sigma^S$ than for $g_\sigma = g_\sigma^L$, and the one π and one ρ exchange potentials do not provide enough

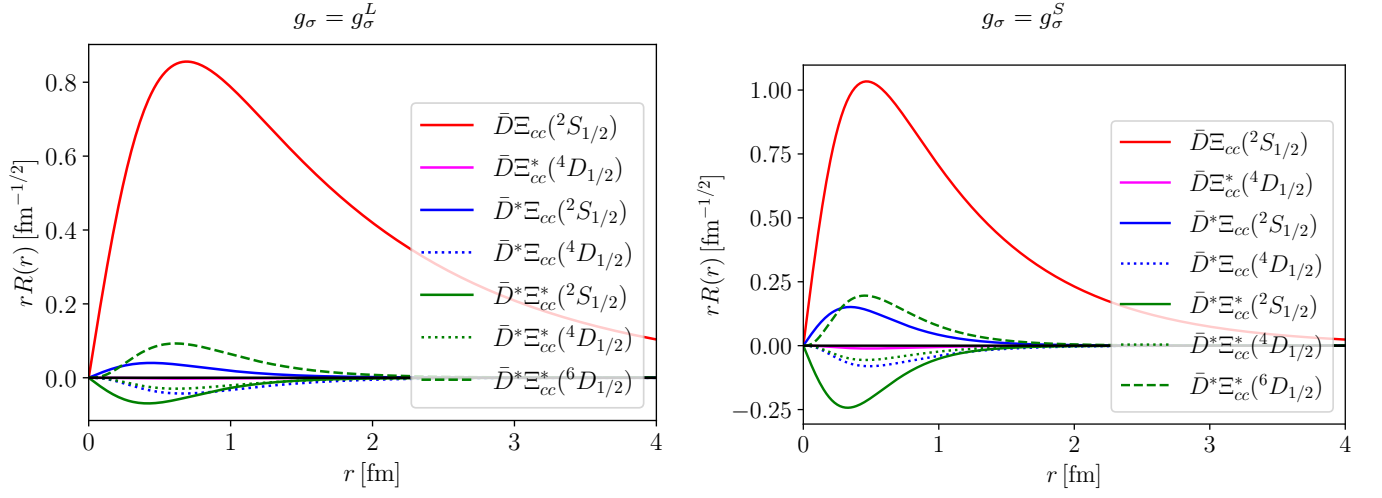


FIG. 2. Wavefunctions of $\bar{D}^{(*)}\Xi_{cc}^{(*)}$ with $I(J^P) = 0(\frac{1}{2}^-)$. The left panel shows the wavefunction of $\bar{D}^{(*)}\Xi_{cc}^{(*)}$ with g_σ^L , while right one shows the wavefunction of $\bar{D}^{(*)}\Xi_{cc}^{(*)}$ with g_σ^S . The red, magenta, blue and green lines show the wavefunctions for $\bar{D}\Xi_{cc}$, $\bar{D}\Xi_{cc}^*$, $\bar{D}^*\Xi_{cc}$ and $\bar{D}^*\Xi_{cc}^*$.

TABLE VI. Channels of $\Xi_{cc}^{(*)}\Xi_{cc}^{(*)}$ with some quantum numbers $I(J^P)$ where I is the isospin. We use $^{2S+1}L_J$ as used in Table III, and $[\Xi_{cc}\Xi_{cc}^*]_{\pm} = \frac{1}{\sqrt{2}}(\Xi_{cc}\Xi_{cc}^* \pm \Xi_{cc}^*\Xi_{cc})$.

$I(J^P)$	Channels
$0(0^+)$	$[\Xi_{cc}\Xi_{cc}^*]_{+}({}^5D_0)$
$1(0^+)$	$\Xi_{cc}\Xi_{cc}({}^1S_0)$, $[\Xi_{cc}\Xi_{cc}^*]_{-}({}^5D_0)$, $\Xi_{cc}^*\Xi_{cc}({}^1S_0, {}^5D_0)$
$0(1^+)$	$\Xi_{cc}\Xi_{cc}({}^3S_1, {}^3D_1)$, $[\Xi_{cc}\Xi_{cc}^*]_{-}({}^3S_1, {}^3D_1)$, $[\Xi_{cc}\Xi_{cc}^*]_{+}({}^5D_1)$, $\Xi_{cc}^*\Xi_{cc}({}^3S_1, {}^3D_1, {}^7D_1, {}^7G_1)$
$1(1^+)$	$[\Xi_{cc}\Xi_{cc}^*]_{+}({}^3S_1, {}^3D_1)$, $[\Xi_{cc}\Xi_{cc}^*]_{-}({}^5D_1)$, $\Xi_{cc}^*\Xi_{cc}({}^5D_1)$
$0(2^+)$	$\Xi_{cc}\Xi_{cc}({}^3D_2)$, $[\Xi_{cc}\Xi_{cc}^*]_{-}({}^3D_2)$, $[\Xi_{cc}\Xi_{cc}^*]_{+}({}^5S_2, {}^5D_2, {}^5G_2)$, $\Xi_{cc}^*\Xi_{cc}({}^3D_2, {}^7D_2, {}^7G_2)$
$1(2^+)$	$\Xi_{cc}\Xi_{cc}({}^1D_2)$, $[\Xi_{cc}\Xi_{cc}^*]_{+}({}^3D_2)$, $[\Xi_{cc}\Xi_{cc}^*]_{-}({}^5S_2, {}^5D_2, {}^5G_2)$, $\Xi_{cc}^*\Xi_{cc}({}^1D_2, {}^5S_2, {}^5D_2, {}^5G_2)$

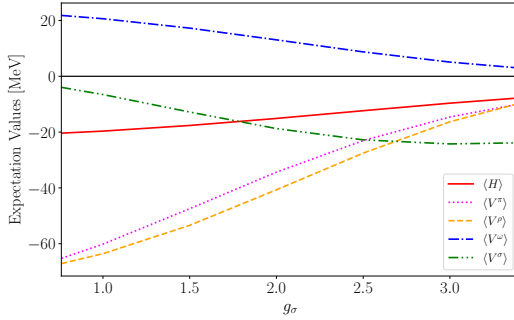


FIG. 3. g_σ dependence of the expectation values of the Hamiltonian and OBEP for $\bar{D}^{(*)}\Xi_{cc}^{(*)}$ with $0(\frac{1}{2}^-)$. The solid line shows the expectation value of the Hamiltonian $\langle H \rangle$, which is equivalent to the binding energy of $\bar{D}^{(*)}\Xi_{cc}^{(*)}$, while the other lines show the expectation values of the one boson exchange potentials denoted by $\langle V^\pi \rangle$, $\langle V^\rho \rangle$, $\langle V^\omega \rangle$ and $\langle V^\sigma \rangle$. The cutoff parameter is determined to reproduce the binding energy of T_{cc} for each g_σ .

TABLE VII. Eigenvalues of $\Xi_{cc}^{(*)}\Xi_{cc}^{(*)}$. The same conventions as Table IV are used.

$I(J^P)$	lowest threshold	$g_\sigma^L = 3.4$	$g_\sigma^S = 0.76$
		$-B$	$E_r - i\frac{\Gamma}{2}$
$0(0^+)$	$\Xi_{cc}\Xi_{cc}^*$	-	-
$1(0^+)$	$\Xi_{cc}\Xi_{cc}$	-2.17	-
		$206 - i\frac{1.58}{2}$	-
$0(1^+)$	$\Xi_{cc}\Xi_{cc}$	-24.7	-67.4
		$76.7 - i\frac{1.19}{2}$	$28.0 - i\frac{1.84}{2}$
		$205 - i\frac{8.19}{2}$	-
$1(1^+)$	$\Xi_{cc}\Xi_{cc}^*$	-0.0594	-
$0(2^+)$	$\Xi_{cc}\Xi_{cc}$	$66.8 - i\frac{2.44}{2}$	$7.31 - i\frac{0.0126}{2}$
$1(2^+)$	$\Xi_{cc}\Xi_{cc}$	$98.1 - i\frac{0.132}{2}$	-
		$211 - i\frac{2.11}{2}$	-

attraction to form a bound state.

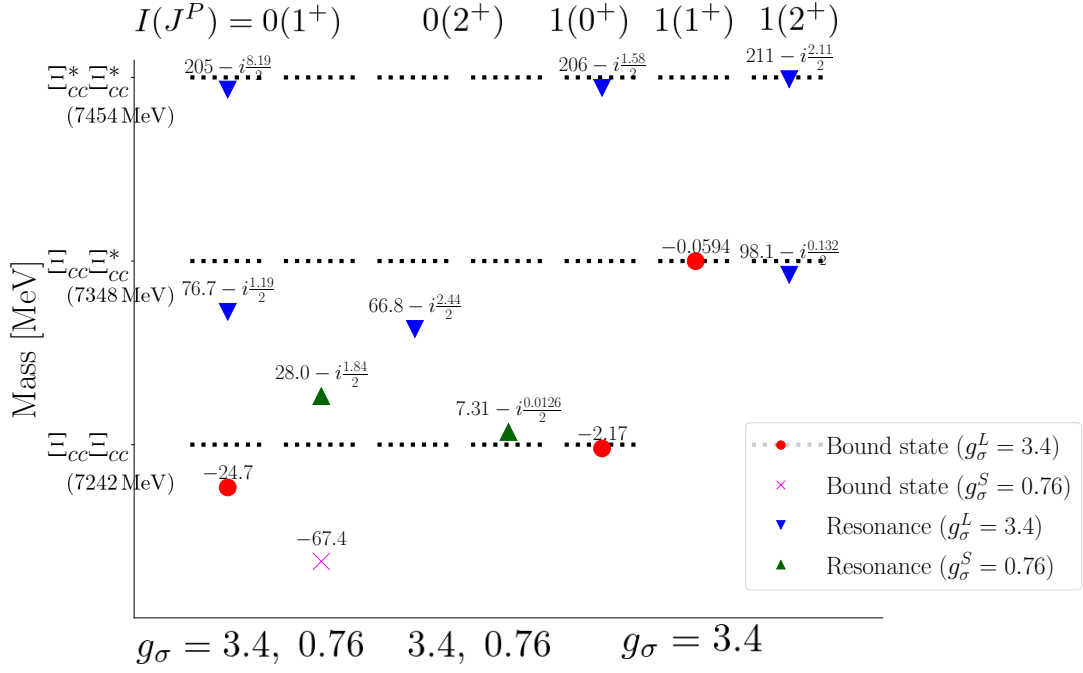


FIG. 4. Masses of $\Xi_{cc}^{(*)}\Xi_{cc}^{(*)}$ with $0(1^+)$, $0(2^+)$, $1(0^+)$, $1(1^+)$ and $1(2^+)$. The same notation as Fig. 1 is used.

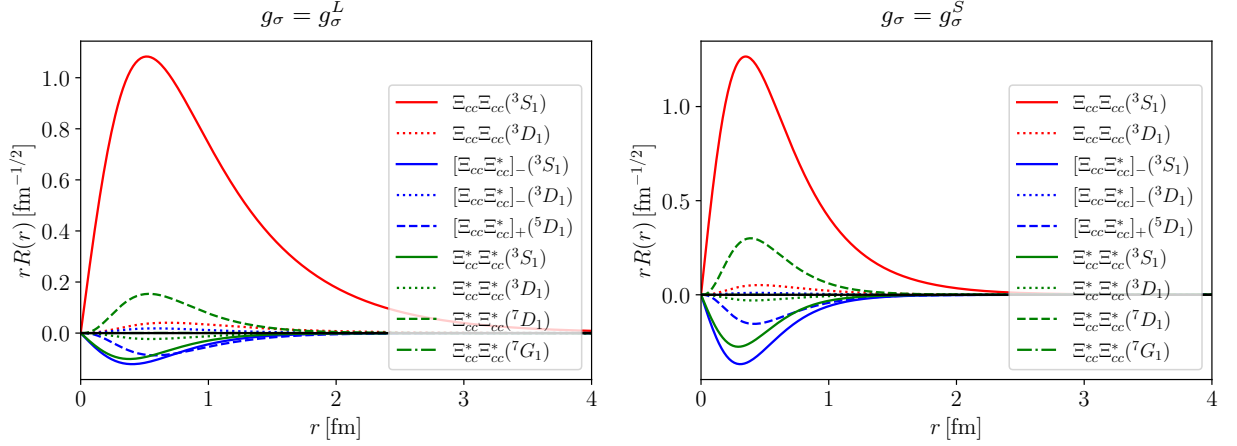


FIG. 5. Wavefunctions of $\Xi_{cc}^{(*)}\Xi_{cc}^{(*)}$ with $I(J^P) = 0(1^+)$. The left panel shows the wavefunction of $\Xi_{cc}^{(*)}\Xi_{cc}^{(*)}$ with g_σ^L , while right one shows the wavefunction of $\Xi_{cc}^{(*)}\Xi_{cc}^{(*)}$ with g_σ^S . The red, blue and green lines show the wavefunctions for $\Xi_{cc}\Xi_{cc}$, $[\Xi_{cc}\Xi_{cc}]_\pm$ and $\Xi_{cc}^*\Xi_{cc}^*$, respectively.

Let us comment on the g_σ dependence of the results. Throughout this work, we have examined the dependence of the results on g_σ . Although all parameter sets reproduce the binding energy of T_{cc} , it is nevertheless intriguing that the resulting predictions differ so significantly. In the future, if $\bar{D}^{(*)}\Xi_{cc}^{(*)}$ and $\Xi_{cc}^{(*)}\Xi_{cc}^{(*)}$ are observed experimentally or studied in lattice QCD, they may provide useful constraints for determining the model parameters.

IV. SUMMARY

In this paper, we have investigated $\bar{D}^{(*)}\Xi_{cc}^{(*)}$ and $\Xi_{cc}^{(*)}\Xi_{cc}^{(*)}$ molecules, respecting the superflavor and heavy quark spin symmetries. These states are superflavor partners of a $D^{(*)}D^{(*)}$ molecule which is a candidate of the structure of T_{cc} , which has been reported by the LHCb in Refs. [10, 12]. Thus, in our previous studies [39, 40], we studied T_{cc} as a $D^{(*)}D^{(*)}$ molecule based on the one boson exchange potential, respecting the heavy quark symmetry. With the help of the superflavor symmetry, we have applied our models for $D^{(*)}D^{(*)}$ to

TABLE VIII. The binding energy B , mixing ratios and root mean squared (r.m.s) distances of $\Xi_{cc}^{(*)}\Xi_{cc}^{(*)}$ with $0(1^+)$ for each case of $g_\sigma = g_\sigma^L$ and $g_\sigma = g_\sigma^S$. The same conventions as Table V are used.

Properties	g_σ	
	$g_\sigma^L = 3.4$	$g_\sigma^S = 0.76$
B	24.7 MeV	67.4 MeV
$\Xi_{cc}\Xi_{cc}(^3S)$	96.6 %	85.9 %
$\Xi_{cc}\Xi_{cc}(^3D)$	0.133 %	0.144 %
$[\Xi_{cc}\Xi_{cc}^*]_{-}(^3S)$	0.834 %	5.92 %
$[\Xi_{cc}\Xi_{cc}^*]_{-}(^3D)$	0.0219 %	0 %
$[\Xi_{cc}\Xi_{cc}^*]_{+}(^5D)$	0.475 %	1.10 %
$\Xi_{cc}^*\Xi_{cc}^*(^3S)$	0.538 %	3.09 %
$\Xi_{cc}^*\Xi_{cc}^*(^3D)$	0.0313 %	0.0402 %
$\Xi_{cc}^*\Xi_{cc}^*(^7D)$	1.34 %	3.80 %
$\Xi_{cc}^*\Xi_{cc}^*(^7G)$	0 %	0 %
r.m.s distance	0.827 fm	0.531 fm

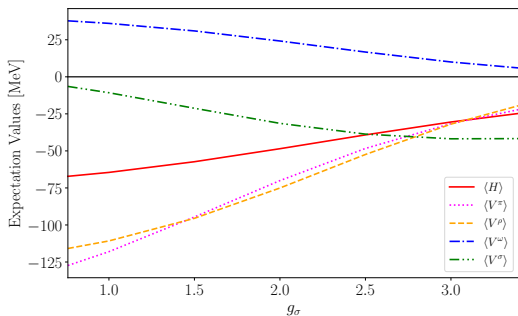


FIG. 6. g_σ dependence of the expectation values of the Hamiltonian and OBEP for $\Xi_{cc}^{(*)}\Xi_{cc}^{(*)}$ with $0(1^+)$. The same notation as Fig. 3 is used.

the $\bar{D}^{(*)}\Xi_{cc}^{(*)}$ and $\Xi_{cc}^{(*)}\Xi_{cc}^{(*)}$ systems, using the same parameters with T_{cc} . Most parameters are determined by the experimental data or Lattice QCD, while the g_σ coupling constant is uncertain. However, we consider two typical values of g_σ : $g_\sigma^L = 3.4$ and $g_\sigma^S = 0.76$. Then, we investigate the g_σ dependence of $\bar{D}^{(*)}\Xi_{cc}^{(*)}$ and $\Xi_{cc}^{(*)}\Xi_{cc}^{(*)}$ states.

First, the cutoff parameter Λ has been determined to reproduce the binding energy of T_{cc} for each g_σ . It was found that the cutoff for $g_\sigma = g_\sigma^S$ is larger than that for $g_\sigma = g_\sigma^L$. This is because for $g_\sigma = g_\sigma^L$ the one σ exchange potential generates enough attractive force to bind T_{cc} , while for $g_\sigma = g_\sigma^S$ the contribution of one σ exchange force becomes weaker, then one π and one ρ exchange potentials should earn enough attractive force.

We have obtained many bound and resonant states of $\bar{D}^{(*)}\Xi_{cc}^{(*)}$ with some quantum numbers. The bound states of $\bar{D}^{(*)}\Xi_{cc}^{(*)}$ were obtained only for $I(J^P) = 0(\frac{1}{2}^-)$. This is because only the $\bar{D}^{(*)}\Xi_{cc}^{(*)}$ state with $J^P = \frac{1}{2}^-$ has S -wave $\bar{D}\Xi_{cc}$ channel. The binding energy of $\bar{D}^{(*)}\Xi_{cc}^{(*)}$ for $g_\sigma = g_\sigma^S$ is smaller than that for $g_\sigma = g_\sigma^L$ because the one π and ρ exchange potentials provide stronger attractive force. For both g_σ cases, the channel of $\bar{D}\Xi_{cc}(^2S)$ is dominant. However, the mixing ratios of the other channels depends on the value of g_σ . For $g_\sigma = g_\sigma^L$ the contributions of the other channels are suppressed, while for $g_\sigma = g_\sigma^S$ some channels are enhanced by the off-diagonal components of one π and one ρ exchange potentials. As for resonant states, many resonances with not only $J^P = \frac{1}{2}^-$ but also $J^P = \frac{3}{2}^-, \frac{5}{2}^-$ were obtained because a large number of $\bar{D}^*\Xi_{cc}^*$ channels contribute to the higher-spin states. All resonances are found to be Feshbach resonances. In the isoscalar states, most resonances for $g_\sigma = g_\sigma^S$ are more deeply bound than those for $g_\sigma = g_\sigma^L$. For the $\bar{D}^*\Xi_{cc}^*$ quasi bound state with $I(J^P) = 0(\frac{3}{2}^-)$, however, we obtain the state only for $g_\sigma = g_\sigma^L$, while no bound state is found for $g_\sigma = g_\sigma^S$. This is because the one π and one ρ exchange potentials cannot generate enough attractive force. For the isovector state, we obtained the resonance only for $I(J^P) = 1(\frac{1}{2}^-)$ with $g_\sigma = g_\sigma^L$, where the one σ exchange potential plays an important role to produce an attraction.

We also have investigated bound and resonant states of $\Xi_{cc}^{(*)}\Xi_{cc}^{(*)}$ with some quantum numbers. As well as the $\bar{D}^{(*)}\Xi_{cc}^{(*)}$ states, many bound and resonant states of $\Xi_{cc}^{(*)}\Xi_{cc}^{(*)}$ were obtained. The $\Xi_{cc}^{(*)}\Xi_{cc}^{(*)}$ states with $I = 0$ were obtained for each g_σ , while the $\Xi_{cc}^{(*)}\Xi_{cc}^{(*)}$ states with $I = 1$ were obtained only for $g_\sigma = g_\sigma^L$. As for the bound states of $\Xi_{cc}^{(*)}\Xi_{cc}^{(*)}$ with $I(J^P) = 0(1^+)$, the binding energy for $g_\sigma = g_\sigma^S$ is larger than that for $g_\sigma = g_\sigma^L$ because the one π and one ρ exchange potentials earn stronger attractive forces. Moreover, all resonances of $\Xi_{cc}^{(*)}\Xi_{cc}^{(*)}$ were found to be Feshbach resonances. As for the $\Xi_{cc}^{(*)}\Xi_{cc}^{(*)}$ resonances with $I = 0$, quasi bound states of $\Xi_{cc}\Xi_{cc}^*$ for $g_\sigma = g_\sigma^S$ are more bound than those for g_σ^L . However, the quasi bound state of $\Xi_{cc}^*\Xi_{cc}^*$ were obtained only for $g_\sigma = g_\sigma^L$.

ACKNOWLEDGEMENT

This work is supported by the Grant-in-Aid for JSPS Fellows No. 25KJ1433 (M.S.) and RCNP Collaboration Research Network program as the project number COREnet-056 (Y.Y.).

[1] S. K. Choi *et al.* (Belle), Observation of a narrow charmonium-like state in exclusive $B^\pm \rightarrow K^\pm \pi^+ \pi^- J/\psi$

decays, Phys. Rev. Lett. **91**, 262001 (2003), arXiv:hep-

- ex/0309032.
- [2] B. Aubert *et al.* (BaBar), Observation of a broad structure in the $\pi^+\pi^-J/\psi$ mass spectrum around 4.26-GeV/ c^2 , Phys. Rev. Lett. **95**, 142001 (2005), arXiv:hep-ex/0506081.
 - [3] C. Z. Yuan *et al.* (Belle), Measurement of $e^+e^- \rightarrow \pi^+\pi^- J/\psi$ cross-section via initial state radiation at Belle, Phys. Rev. Lett. **99**, 182004 (2007), arXiv:0707.2541 [hep-ex].
 - [4] S. K. Choi *et al.* (Belle), Observation of a resonance-like structure in the $\pi^{\pm}\psi'$ mass distribution in exclusive $B \rightarrow K\pi^{\pm}\psi'$ decays, Phys. Rev. Lett. **100**, 142001 (2008), arXiv:0708.1790 [hep-ex].
 - [5] B. Aubert *et al.* (BaBar), Search for the Z(4430)-at BABAR, Phys. Rev. D **79**, 112001 (2009), arXiv:0811.0564 [hep-ex].
 - [6] R. Aaij *et al.* (LHCb), Observation of $J/\psi p$ Resonances Consistent with Pentaquark States in $\Lambda_b^0 \rightarrow J/\psi K^- p$ Decays, Phys. Rev. Lett. **115**, 072001 (2015), arXiv:1507.03414 [hep-ex].
 - [7] R. Aaij *et al.* (LHCb), Observation of a narrow pentaquark state, $P_c(4312)^+$, and of two-peak structure of the $P_c(4450)^+$, Phys. Rev. Lett. **122**, 222001 (2019), arXiv:1904.03947 [hep-ex].
 - [8] R. Aaij *et al.* (LHCb), Observation of structure in the J/ψ -pair mass spectrum, Sci. Bull. **65**, 1983 (2020), arXiv:2006.16957 [hep-ex].
 - [9] R. Aaij *et al.* (LHCb), Evidence of a $J/\psi\Lambda$ structure and observation of excited Ξ^- states in the $\Xi_b^- \rightarrow J/\psi\Lambda K^-$ decay, Sci. Bull. **66**, 1278 (2021), arXiv:2012.10380 [hep-ex].
 - [10] R. Aaij *et al.* (LHCb), Observation of an exotic narrow doubly charmed tetraquark, Nature Phys. **18**, 751 (2022), arXiv:2109.01038 [hep-ex].
 - [11] R. Aaij *et al.* (LHCb), Study of the doubly charmed tetraquark T_{cc}^+ , Nature Commun. **13**, 3351 (2022), arXiv:2109.01056 [hep-ex].
 - [12] R. Aaij *et al.* (LHCb), Evidence for a new structure in the $J/\psi p$ and $J/\psi\bar{p}$ systems in $B_s^0 \rightarrow J/\psi p\bar{p}$ decays, Phys. Rev. Lett. **128**, 062001 (2022), arXiv:2108.04720 [hep-ex].
 - [13] M. Ablikim *et al.* (BESIII), Observation of a Near-Threshold Structure in the K^+ Recoil-Mass Spectra in $e^+e^- \rightarrow K^+(D_s^- D^{*0} + D_s^{*-} D^0)$, Phys. Rev. Lett. **126**, 102001 (2021), arXiv:2011.07855 [hep-ex].
 - [14] N. A. Tornqvist, From the deuteron to deusons, an analysis of deuteron - like meson meson bound states, Z. Phys. C **61**, 525 (1994), arXiv:hep-ph/9310247.
 - [15] F.-K. Guo, C. Hanhart, U.-G. Meißner, Q. Wang, Q. Zhao, and B.-S. Zou, Hadronic molecules, Rev. Mod. Phys. **90**, 015004 (2018), [Erratum: Rev.Mod.Phys. 94, 029901 (2022)], arXiv:1705.00141 [hep-ph].
 - [16] R. Machleidt, K. Holinde, and C. Elster, The Bonn Meson Exchange Model for the Nucleon Nucleon Interaction, Phys. Rept. **149**, 1 (1987).
 - [17] R. Machleidt, The High precision, charge dependent Bonn nucleon-nucleon potential (CD-Bonn), Phys. Rev. C **63**, 024001 (2001), arXiv:nucl-th/0006014.
 - [18] M. Oka and K. Yazaki, Short Range Part of Baryon Baryon Interaction in a Quark Model. 1. Formulation, Prog. Theor. Phys. **66**, 556 (1981).
 - [19] M. Oka and K. Yazaki, Short Range Part of Baryon Baryon Interaction in a Quark Model. 2. Numerical Results for S-Wave, Prog. Theor. Phys. **66**, 572 (1981).
 - [20] M. Oka, K. Shimizu, and K. Yazaki, Quark cluster model of baryon baryon interaction, Prog. Theor. Phys. Suppl. **137**, 1 (2000).
 - [21] T. Sekihara and T. Hashiguchi, Reexamination of the short-range baryon-baryon potentials in the constituent quark model, Phys. Rev. C **108**, 065202 (2023), arXiv:2304.13877 [nucl-th].
 - [22] S. Aoki, T. Hatsuda, and N. Ishii, Theoretical Foundation of the Nuclear Force in QCD and its applications to Central and Tensor Forces in Quenched Lattice QCD Simulations, Prog. Theor. Phys. **123**, 89 (2010), arXiv:0909.5585 [hep-lat].
 - [23] T. Inoue, N. Ishii, S. Aoki, T. Doi, T. Hatsuda, Y. Ikeda, K. Murano, H. Nemura, and K. Sasaki (HAL QCD), Bound H-dibaryon in Flavor SU(3) Limit of Lattice QCD, Phys. Rev. Lett. **106**, 162002 (2011), arXiv:1012.5928 [hep-lat].
 - [24] N. Ishii, S. Aoki, T. Doi, T. Hatsuda, Y. Ikeda, T. Inoue, K. Murano, H. Nemura, and K. Sasaki (HAL QCD), Hadron-hadron interactions from imaginary-time Nambu-Bethe-Salpeter wave function on the lattice, Phys. Lett. B **712**, 437 (2012), arXiv:1203.3642 [hep-lat].
 - [25] Y. Lyu, S. Aoki, T. Doi, T. Hatsuda, Y. Ikeda, and J. Meng, Doubly Charmed Tetraquark Tcc+ from Lattice QCD near Physical Point, Phys. Rev. Lett. **131**, 161901 (2023), arXiv:2302.04505 [hep-lat].
 - [26] M. Neubert, Heavy quark symmetry, Phys. Rept. **245**, 259 (1994), arXiv:hep-ph/9306320.
 - [27] B. Grinstein, An Introduction to heavy mesons, in *6th Mexican School of Particles and Fields* (1995) pp. 122–184, arXiv:hep-ph/9508227.
 - [28] R. Casalbuoni, A. Deandrea, N. Di Bartolomeo, R. Gatto, F. Feruglio, and G. Nardulli, Phenomenology of heavy meson chiral Lagrangians, Phys. Rept. **281**, 145 (1997), arXiv:hep-ph/9605342.
 - [29] H. Georgi and M. B. Wise, Superflavor Symmetry for Heavy Particles, Phys. Lett. B **243**, 279 (1990).
 - [30] M. J. Savage and M. B. Wise, Spectrum of baryons with two heavy quarks, Phys. Lett. B **248**, 177 (1990).
 - [31] S. Fleming and T. Mehen, Doubly heavy baryons, heavy quark-diquark symmetry and NRQCD, Phys. Rev. D **73**, 034502 (2006), arXiv:hep-ph/0509313.
 - [32] S. Ohkoda, Y. Yamaguchi, S. Yasui, K. Sudoh, and A. Hosaka, Exotic mesons with double charm and bottom flavor, Phys. Rev. D **86**, 034019 (2012), arXiv:1202.0760 [hep-ph].
 - [33] N. Li, Z.-F. Sun, X. Liu, and S.-L. Zhu, Coupled-channel analysis of the possible $D^{(*)}D^{(*)}$, $\bar{B}^{(*)}\bar{B}^{(*)}$ and $D^{(*)}\bar{B}^{(*)}$ molecular states, Phys. Rev. D **88**, 114008 (2013), arXiv:1211.5007 [hep-ph].
 - [34] H.-X. Chen, W. Chen, X. Liu, Y.-R. Liu, and S.-L. Zhu, An updated review of the new hadron states, Rept. Prog. Phys. **86**, 026201 (2023), arXiv:2204.02649 [hep-ph].
 - [35] F.-L. Wang, R. Chen, and X. Liu, A new group of doubly charmed molecule with T-doublet charmed meson pair, Phys. Lett. B **835**, 137502 (2022), arXiv:2111.00208 [hep-ph].
 - [36] F.-L. Wang and X. Liu, Investigating new type of doubly charmed molecular tetraquarks composed of charmed mesons in the H and T doublets, Phys. Rev. D **104**, 094030 (2021), arXiv:2108.09925 [hep-ph].
 - [37] H. Ren, F. Wu, and R. Zhu, Hadronic Molecule Interpretation of Tcc+ and Its Beauty Partners, Adv. High

- Energy Phys. **2022**, 9103031 (2022), arXiv:2109.02531 [hep-ph].
- [38] T. Asanuma, Y. Yamaguchi, and M. Harada, Analysis of DD^* and $D^-(*)\Xi_{cc}^*$ molecule by one boson exchange model based on heavy quark symmetry, Phys. Rev. D **110**, 074030 (2024), arXiv:2311.04695 [hep-ph].
- [39] M. Sakai and Y. Yamaguchi, Analysis of T_{cc} and T_{bb} based on the hadronic molecular model and their spin multiplets, Phys. Rev. D **109**, 054016 (2024), arXiv:2312.08663 [hep-ph].
- [40] M. Sakai and Y. Yamaguchi, Analysis of bound and resonant states of doubly heavy tetraquarks with spin $J \leq 2$, Phys. Rev. D **112**, 034038 (2025), arXiv:2503.11134 [hep-ph].
- [41] Y. Ikeda, B. Charron, S. Aoki, T. Doi, T. Hatsuda, T. Inoue, N. Ishii, K. Murano, H. Nemura, and K. Sasaki, Charmed tetraquarks T_{cc} and T_{cs} from dynamical lattice QCD simulations, Phys. Lett. B **729**, 85 (2014), arXiv:1311.6214 [hep-lat].
- [42] M. Padmanath and S. Prelovsek, Signature of a Doubly Charm Tetraquark Pole in DD^* Scattering on the Lattice, Phys. Rev. Lett. **129**, 032002 (2022), arXiv:2202.10110 [hep-lat].
- [43] M. Nagatsuka and S. Sasaki, Lattice study of scattering phase shifts for DD^* and BB^* systems using twisted boundary conditions: Search for bound state formation, Phys. Rev. D **112**, 114510 (2025), arXiv:2507.20712 [hep-lat].
- [44] B. Grinstein, E. E. Jenkins, A. V. Manohar, M. J. Savage, and M. B. Wise, Chiral perturbation theory for $f D(s) / f D$ and $B B(s) / B B$, Nucl. Phys. B **380**, 369 (1992), arXiv:hep-ph/9204207.
- [45] Y. Yamaguchi, S. Yasui, and A. Hosaka, Open charm and bottom meson-nucleon potentials à la the nuclear force, Phys. Rev. D **106**, 094001 (2022), arXiv:2206.01921 [hep-ph].
- [46] S. Ahmed *et al.* (CLEO), First measurement of $\Gamma(D^{*+})$, Phys. Rev. Lett. **87**, 251801 (2001), arXiv:hep-ex/0108013.
- [47] M.-Z. Liu, T.-W. Wu, M. Pavon Valderrama, J.-J. Xie, and L.-S. Geng, Heavy-quark spin and flavor symmetry partners of the $X(3872)$ revisited: What can we learn from the one boson exchange model?, Phys. Rev. D **99**, 094018 (2019), arXiv:1902.03044 [hep-ph].
- [48] C. Isola, M. Ladisa, G. Nardulli, and P. Santorelli, Charming penguins in $B \rightarrow K^* \pi$, $K(\rho, \omega, \phi)$ decays, Phys. Rev. D **68**, 114001 (2003), arXiv:hep-ph/0307367.
- [49] W. A. Bardeen, E. J. Eichten, and C. T. Hill, Chiral Multiplets of Heavy - Light Mesons, Phys. Rev. D **68**, 054024 (2003), arXiv:hep-ph/0305049.
- [50] X. Liu, Y.-R. Liu, W.-Z. Deng, and S.-L. Zhu, $Z^+(4430)$ as a $D(1)$ -prime D^* ($D(1) D^*$) molecular state, Phys. Rev. D **77**, 094015 (2008), arXiv:0803.1295 [hep-ph].
- [51] J. Hu and T. Mehen, Chiral Lagrangian with heavy quark-diquark symmetry, Phys. Rev. D **73**, 054003 (2006), arXiv:hep-ph/0511321.
- [52] S. Navas *et al.* (Particle Data Group), Review of particle physics, Phys. Rev. D **110**, 030001 (2024).
- [53] E. Hiyama, Y. Kino, and M. Kamimura, Gaussian expansion method for few-body systems, Prog. Part. Nucl. Phys. **51**, 223 (2003).
- [54] E. Hiyama and M. Kamimura, Study of various few-body systems using Gaussian expansion method (GEM), Front. Phys. (Beijing) **13**, 132106 (2018), arXiv:1809.02619 [nucl-th].
- [55] R. Suzuki, T. Myo, and K. Kato, Level density in complex scaling method, AIP Conf. Proc. **768**, 455 (2005), arXiv:nucl-th/0502012.
- [56] T. Myo, Y. Kikuchi, H. Masui, and K. Katō, Recent development of complex scaling method for many-body resonances and continua in light nuclei, Prog. Part. Nucl. Phys. **79**, 1 (2014), arXiv:1410.4356 [nucl-th].
- [57] T. Myo and K. Kato, Complex scaling: Physics of unbound light nuclei and perspective, PTEP **2020**, 12A101 (2020), arXiv:2007.12172 [nucl-th].